We are IntechOpen,
the world's leading publisher of
Open Access books
Built by scientists, for scientists

4,800
Open access books available

122,000
International authors and editors

135M
Downloads

Our authors are among the

154
Countries delivered to

TOP 1%
most cited scientists

12.2%
Contributors from top 500 universities

CLARIVATE ANALYTICS
BOOK CITATION INDEX
INDEXED

WEB OF SCIENCE™

Selection of our books indexed in the Book Citation Index
in Web of Science™ Core Collection (BKCI)

Interested in publishing with us?
Contact book.department@intechopen.com

Numbers displayed above are based on latest data collected.
For more information visit www.intechopen.com

Sintering and Heat Treatment of Titanium Alloys by Pulsed Electric Current Sintering

F. Zhang, Y. Quan, M. Reich, O. Kessler and E. Burkel

Additional information is available at the end of the chapter

1. Introduction

Pulsed electric current sintering (PECS), commonly also defined as spark plasma sintering (SPS), field assisted sintering (FAST) is a novel pressure assisted pulsed electric current sintering process utilizing ON-OFF DC pulse energizing. Due to the repeated application of the ON-OFF DC pulsed voltage and current in powder materials, the spark discharge point and the Joule heating point (local high temperature-state) are transferred and dispersed to the overall specimen [1]. The PECS process is based on the electrical spark discharge phenomenon: a high energetic, low voltage spark pulse current momentarily generating high localized temperatures, from several to ten thousand degrees between the particles resulting in high thermal and electrolytic diffusion [1, 2].

Because of the time- and cost- effective manufacturing which it permits, sinter hardening has come into being a process of high importance in powder metallurgy (PM) in the past years [3]. It is a hardening method applicable only for PM parts in which the parts are sintered and quenched directly after the sintering step saving energy and costs connected to conventional hardening where the parts have to be reheated to hardening temperature [3, 4]. Furthermore, sinter hardening is performed by gas quenching instead of oil quenching being beneficial in terms of dimensional stability and cleanliness of the specimen. Due to poor thermal transfer characteristics (lower cooling rate) of gases under normal conditions, they have to be optimized by proper adjustment of gas pressure and flow speed. In principle, gas quenching can be performed in two ways [5-8], namely: at low or atmosphere pressure with high gas velocity or at high pressure with limited gas velocities. The first part of this chapter will focus on new modifications of the PECS technique. The PECS has been modified and integrated with a novel gas quenching system. The PECS in vacuum status was quenched with high-velocity nitrogen gas. The Al-2024 alloy and ALSI-303 stainless steel have been

used for cooling power measurement and numerical simulation of the quenching process. The $\alpha+\beta$ Ti6Al4V alloy has been used as a model material to study the effects of the cooling rate on the microstructure and mechanical properties of the sintered alloy.

The second part of this chapter will focus on the preparation of Ti6Al4V foams by the PECS with a post heat treatment. Since, the mismatches of the Young's moduli of the human bones and the Ti6Al4V implants lead to stress shielding effects responsible for bone resorption and eventual implant loosening. Porous structures are expected to provide a better interaction with the bones. The fabrication of porous Ti alloy with standard techniques is difficult due to the high melting point and the extreme chemical affinity to atmospheric gases like oxygen, hydrogen, and nitrogen, especially at elevated temperatures. Currently, the fabrication of porous Ti alloy is mainly focused on powder metallurgy approaches [9]. The use of space holder materials allows a simple and accurate control of pore fraction, shape and connectivity in titanium alloys. Open-celled pure titanium foams were fabricated by vacuum hot pressing of a blend of Ti and NaCl spacer followed by NaCl removal in water [10]. However, the Ti6Al4V/NaCl mixture is difficult to be densified by the hot pressing due to the higher creep resistance of this alloy at 790 °C [10]. Promising approach to produce Ti alloys is the pulsed electric current sintering process. The PECS can easily sinter Ti and Ti alloy powders applying pressure and high pulsed DC currents. Thus the local surfaces of the particles melt, allowing junctions to be formed between particles in contact. The combination of the PECS technique with a NaCl space holder was used in porous pure Ti to fabricate macroporous Ti foams with controlled architectures recently [11]. This indicated that the PECS may be able to fabricate Ti6Al4V foams from the Ti6Al4V/NaCl powder mixture. The microstructures, mechanical properties and cell proliferation properties of the fabricated foams were investigated. Some other methods for preparation of Ti alloy foams by the PECS were also introduced.

2. Materials and methods

- The Ti6Al4V powder with a particle size about 20 μm was obtained from TLS Technik GmbH & Co, Germany. The element contents have aluminum 5.9%, vanadium 3.9%, carbon 0.01%, oxygen 0.12%, iron 0.19%, nitrogen 0.01% and hydrogen 0.004% (wt.%). The space holder materials (NaCl, Cu, Mg) for preparation of Ti6Al4V foams with 99.0% purity were obtained from Alfa Aesar and sieved in the range of 50 to 250 μm.

- The PECS experiments were conducted using a Model HP D-125 FCT spark plasma sintering system (FCT systeme GmbH, Rauenstein, Germany) installed at the Tycho Sinter Lab in the University of Rostock. The temperatures in different sites of the samples were measured by Pyrometer and thermal couples.

- The numerical simulations used a rotation-symmetric finite-element-model considering the axial symmetry by software MSC.MARC 2010.1.0.

- The hardness of the polished samples was measured with a SHIMADAZU Micro Hardness tester HMV. The compressive strength and ductility under compressive load was

performed according to DIN 50106 on an Instron 8502 testing machine at room temperature with a compression speed of 0.5 mm/min.

- The polished metallographic samples were etched by Weck's reagent (2 g ammonium acid, 100 ml distilled water, 50 ml alcohol) for 20 seconds and subjected to optical microscopy to observe microstructure morphologies. The fracture surface of the compressed samples was analyzed using scanning electron microscope (SEM, Zeiss Supra 25, Germany) at 20 keV. The Ti6Al4V foam architecture was examined by using X-ray microcomputed tomography (Micro-CT, GE, USA). The phase composition was analyzed using high energy synchrotron radiation (42.58 keV) at Beamline P02.2 (DESY/ PETRA III).

- The human osteoblast-like cell line MG-63 (ATCC, CRL-1427, LGC Promochem, Wesel, Germany) was used for the evaluation of the cellular acceptance of the surfaces

## 3. Ti6Al4V alloys prepared by PECS with a gas quenching system

3.1. Gas quenching system and cooling power

Figure 1 shows the image of the gas quenching system in the PECS. In the system, six nozzles in one group and eight groups up to 48 nozzles are arranged rotationally symmetric around the sintered component. The gas is distributed evenly on all nozzles. The gas nozzle field is positioned inside the PECS chamber and quenches the sintered component together with the graphite tool directly after sintering without any movement of the component [12]. The temperature is measured by a central pyrometer with a focus point at the bottom of the central borehole of the graphite up-punch and thermal couples. The Al alloy and steel cylinders (ϕ60 mm) were heated and quenched in the PECS as dense materials without sintering, to study the quenching power without sintering influence. The Ti6Al4V powders were pressed into a ϕ40 mm graphite die, and sintered at 850 °C and 50 MPa in vacuum. A heating rate of 100 K/min was adopted, and the sintering process lasted typically 6 min. The applied direct current for PECS was 1000-2000 A with pulse duration of 10 ms and an interval of 5 ms. Before cooling, the PECS furnace was flooded with argon gas keeping the sintering temperature. Afterwards, it was quenched from 850 °C using room temperature nitrogen gas at very high flowing rate of 8000 l/min out of the nozzles.

In Figure 2 the cooling curve in the core of the Al 2024-sample surrounded by the graphite form during gas quenching from 480 °C is compared to the curves that were achieved by natural cooling with or without flooding the sinter chamber. The gas quenching exerts a considerable influence, so that the Al alloy cools down to 200 °C after flooding the vacuum chamber more than twice as fast as without being quenched. A maximum cooling rate of 2.0 K/s is reached during quenching in contrast to 0.5 K/s during natural cooling. Figure 3 shows that the cooling process of the steel sample from 850 °C is affected by the gas nozzle field quenching, too. With surrounding graphite form the sample cooled down to 200 °C thrice as fast as naturally cooled after flooding the vacuum chamber. By gas quenching maximum cooling rates of 2.6 K/s with graphite form were reached, whereas a natural cooling affects only maximum cooling rates of 0.9 K/s with graphite form.

Figure 1. The image of the gas quenching system in the pulsed electric current sintering.
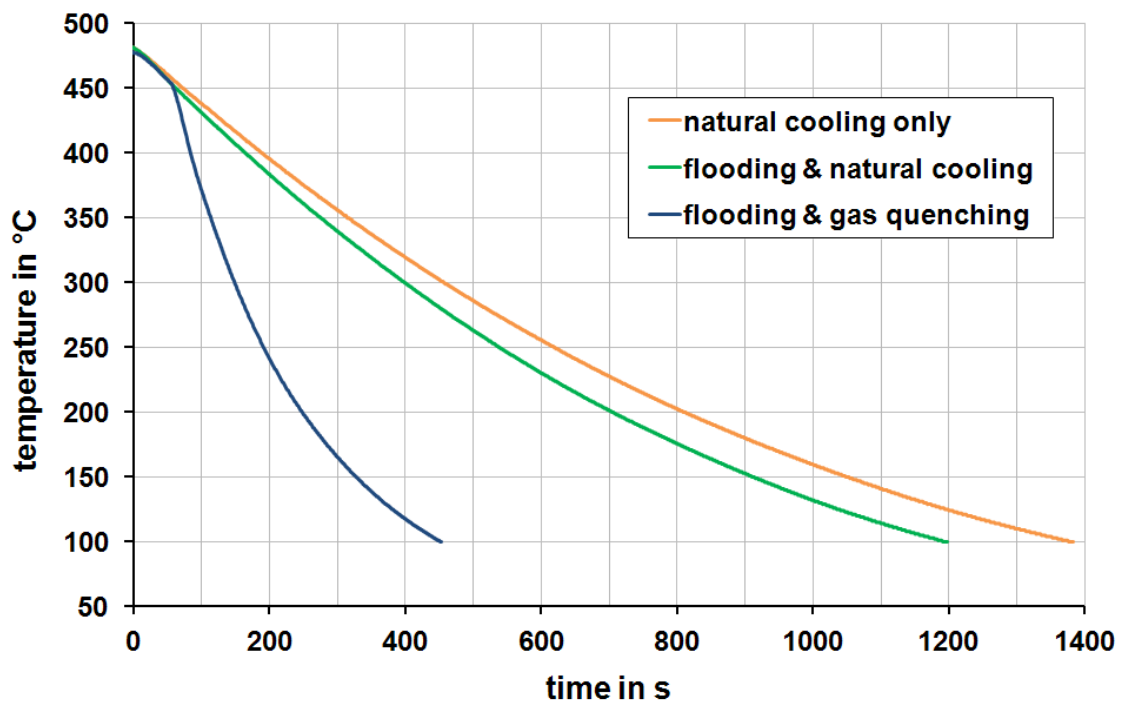
Figure 2. Measured cooling curve in the core of an Al-2024 sample surrounded by the graphite form during gas quenching with 8000 l/min (nitrogen) compared to natural cooling
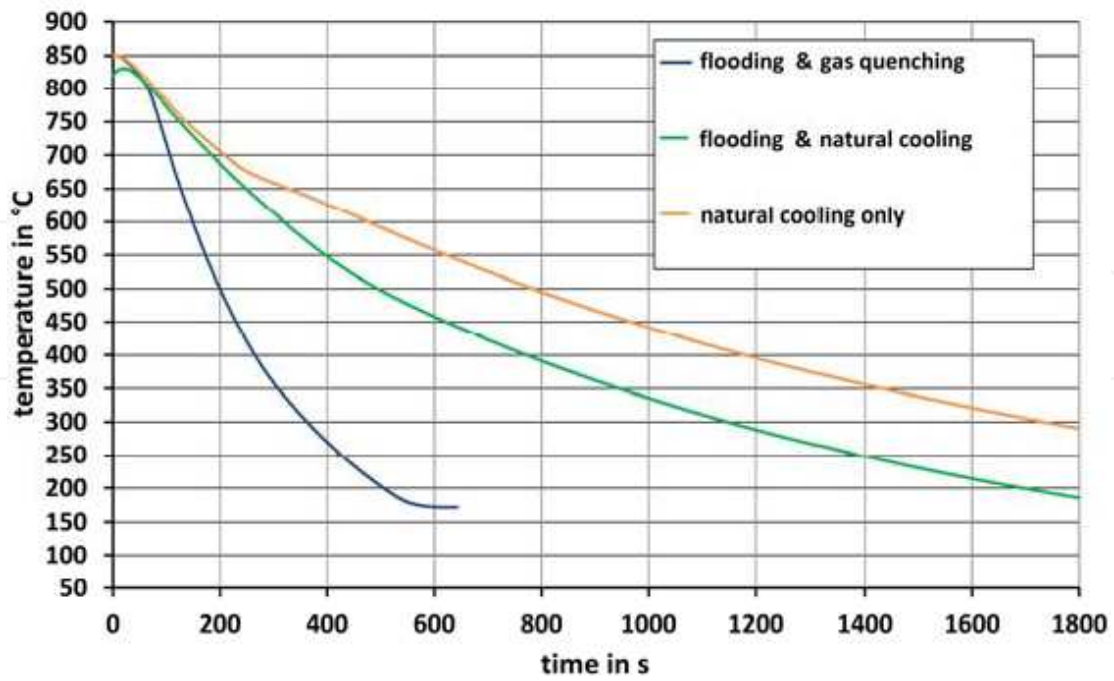
Figure 3. Measured cooling curves in the core of an AISI 303 stainless steel sample during gas quenching with 8000 (nitrogen) compared to natural cooling without the graphite form
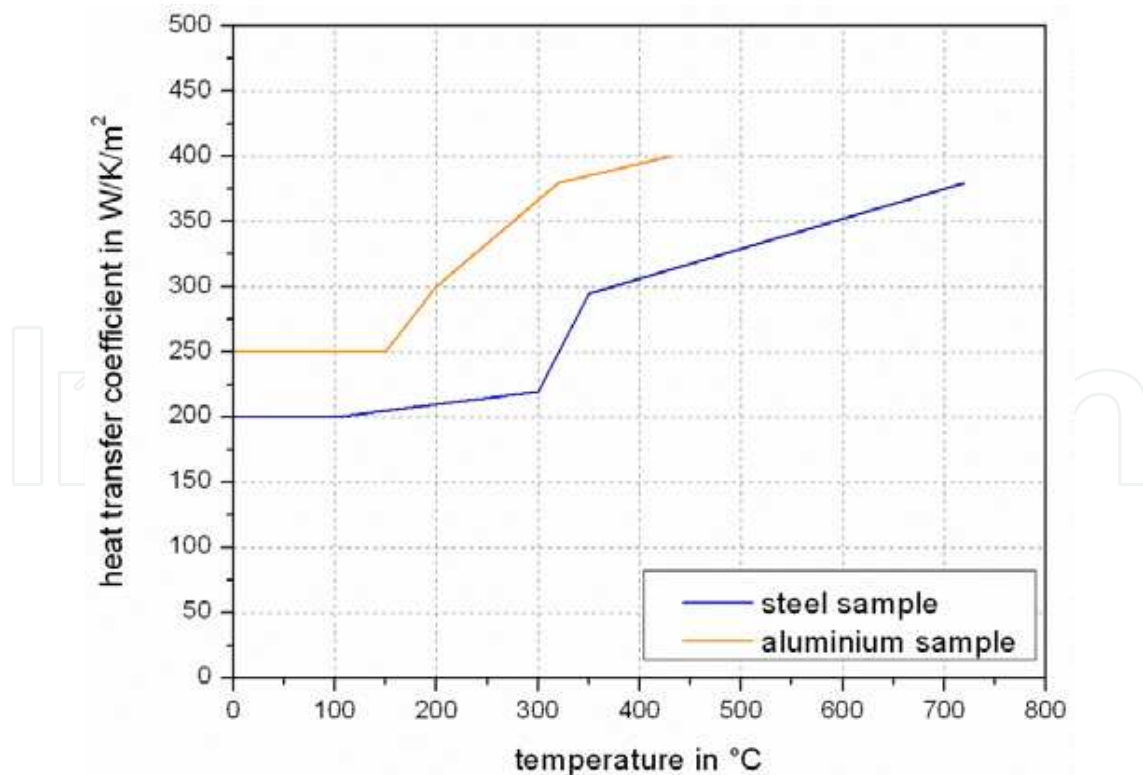
Figure 4. Calculated heat transfer coefficient of aluminium and steel samples.

From these cooling curves, heat transfer coefficients have been determined by inverse thermal simulation. Thereby the thermophysical properties of the surrounding graphite die have been considered. The determined coefficient for the aluminium and the steel sample are set out in Figure 4. Over the process time, the gas nozzle filed loses quench intensity. The heat transfer coefficient falls from about 400 W/(m²K) to the half of initial value.

Figure 5 contains the results of the FEM-simulation for the quenching of the steel sample after 100 s. The temperature distribution reflects the different thermal behavior of steel and graphite. The heat of the sample is discharged considerably through the surface of the sinter form being cooled by gas nozzle field. However, only a small proportion of the sample heat dissipates in the massive stamps.
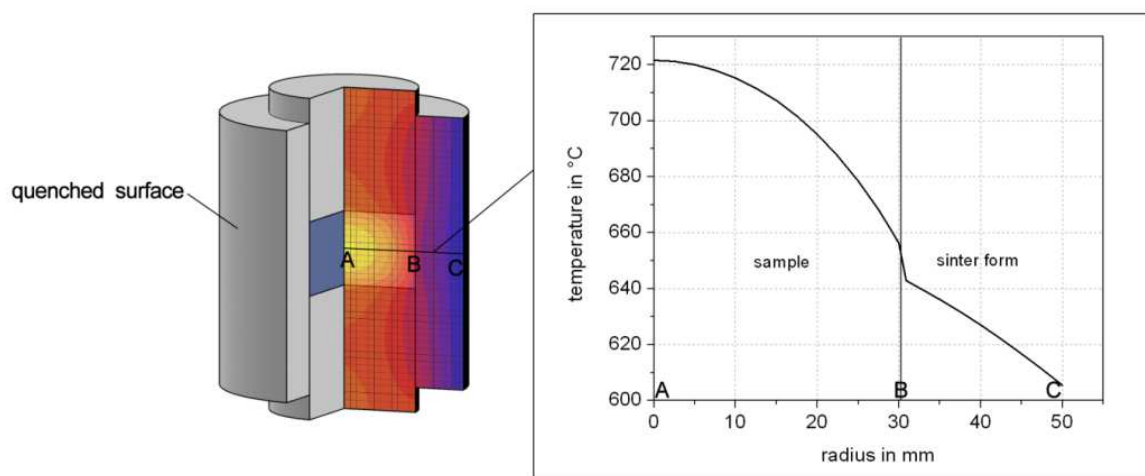
Figure 5. Quenching simulation results of steel sample, temperature distribution after 100 s.

Various cooling rates can be achieved by changing the thickness of the graphite die or the flowing rate of the nitrogen gas (0-8000 l/min). In this study, various cooling rates of the Ti6Al4V alloy are obtained with altering the thickness of the dies. The sample dimensions are 40 mm in diameter and 10-12 mm in height. Figure 6 shows the temperature-time cooling curve of the sintered Ti6Al4V alloys with various cooling rates. Below 400 ºC, the pyrometer cannot measure the temperature of the sample. From the cooling curves sample mean cooling rates of samples 1.6 K/s, 4.8 K/s, 5.6 K/s and 6.9 K/s with an uncertainty of 0.1 K/s were derived. The cooling rate 1.6 K/s was achieved with a 20 mm thick graphite die with a natural cooling, 4.8 K/s with the 20 mm die with gas quenching, and 5.6 K/s with the 10 mm die, also with gas quenching. The rate of 6.9 K/s was achieved in two steps. Hereby, the powder sample was firstly sintered in the PECS at 500 ºC for 5 min at 50 MPa in die to get a 70-80% relative density, and then heated to a sintering temperature of 850 ºC without die to get full density and directly gas quenched to the specimen, later on.
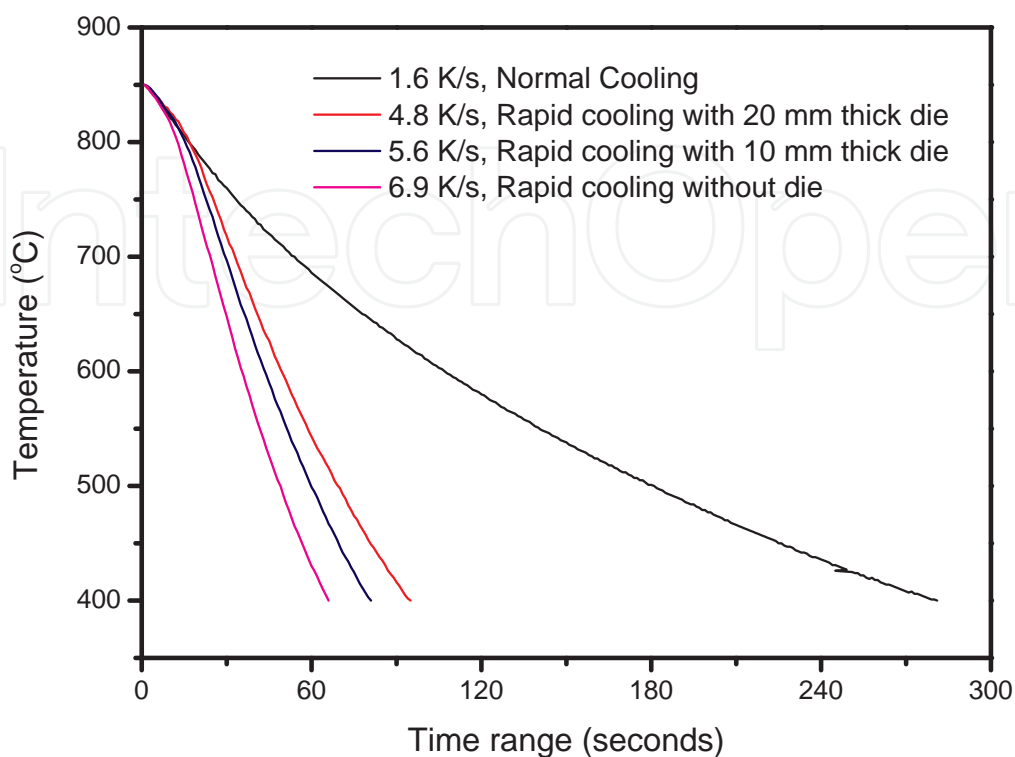
Figure 6. The cooling curves of pyrometer temperature as a function of time showing the temperatures in the center of the Ti6Al4V samples with various quenching rates.

3.2. Mechanical properties of the gas quenched Ti6Al4V alloys

Figure 7 shows the hardness (HV1) of the sinter hardened Ti6Al4V alloy with various cooling rates. The naturally cooled sample with the cooling rate of 1.6 K/s has hardness of 327±8. The gas quenched samples show hardness of 337±7, 342±4.4 and 353±3.6 for cooling rate of 4.8, 5.6 and 6.9 K/s, respectively. The hardness increases with higher cooling rate. Thus, sinter hardening of the Ti6Al4V alloys has been realized by the PECS with gas quenching.

Figure 8 shows the effects of cooling rate on the ultimate compressive strength and ductility of the Ti6Al4V alloys. The ultimate compressive strength goes up with the increase of the cooling rate. The samples of natural cooling rate 1.6 K/s show the ultimate compressive strength of 1578±80 MPa. At a cooling rate of 4.8 K/s, it reached to 1723±63 MPa. At 5.6 K/s cooling rate, it is increased to 1775±70 MPa and at 6.9 K/s, it rises to 1832±43 MPa. The rapid cooling has increased the ultimate compressive strength of the Ti6Al4V alloy. The ductility increased with higher cooling rate. The samples with natural cooling rate 1.6 K/s show a ductility of 25.7±2.3 %. At a cooling rate of 4.8 K/s, it reaches to 27.9±2.4 %, at 5.63 K/s to 29.5±2 %, and at 6.9 K/s to 34.0±2.7 %. The rapid cooling in the PECS has enhanced the ductility of the Ti6Al4V alloy.
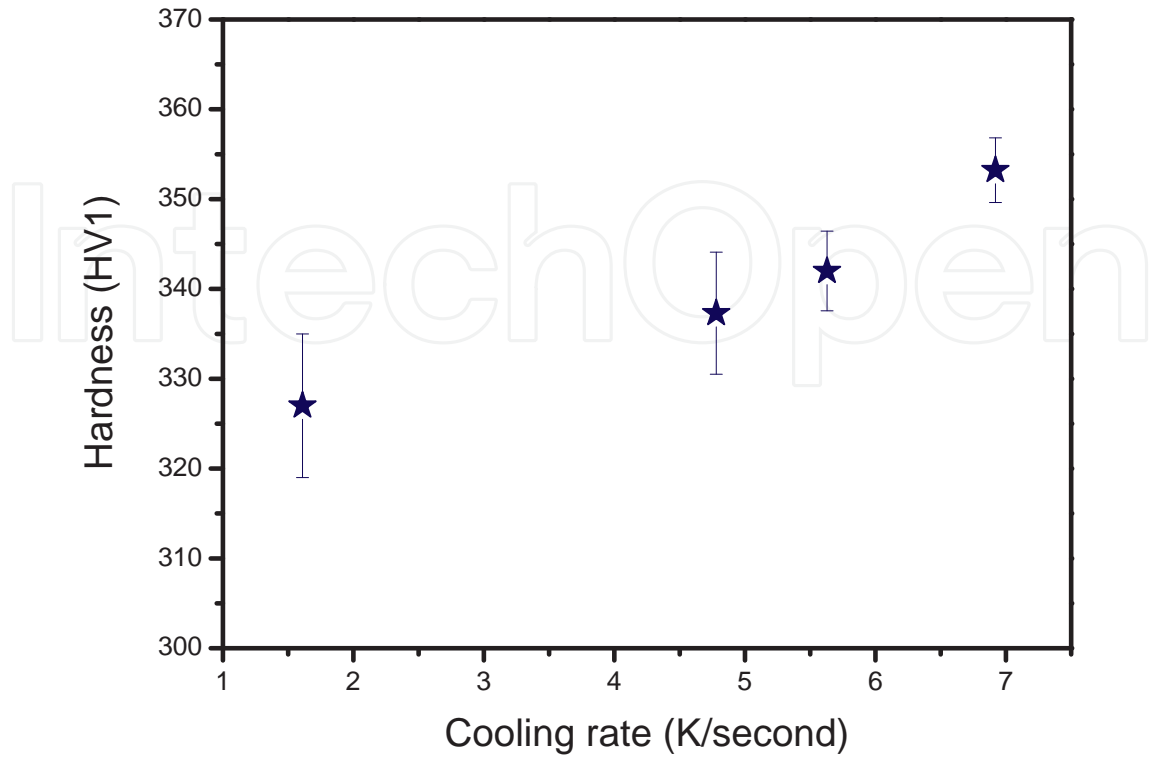
Figure 7. Hardness (HV1) of the Ti6Al4V alloys with various cooling rates.
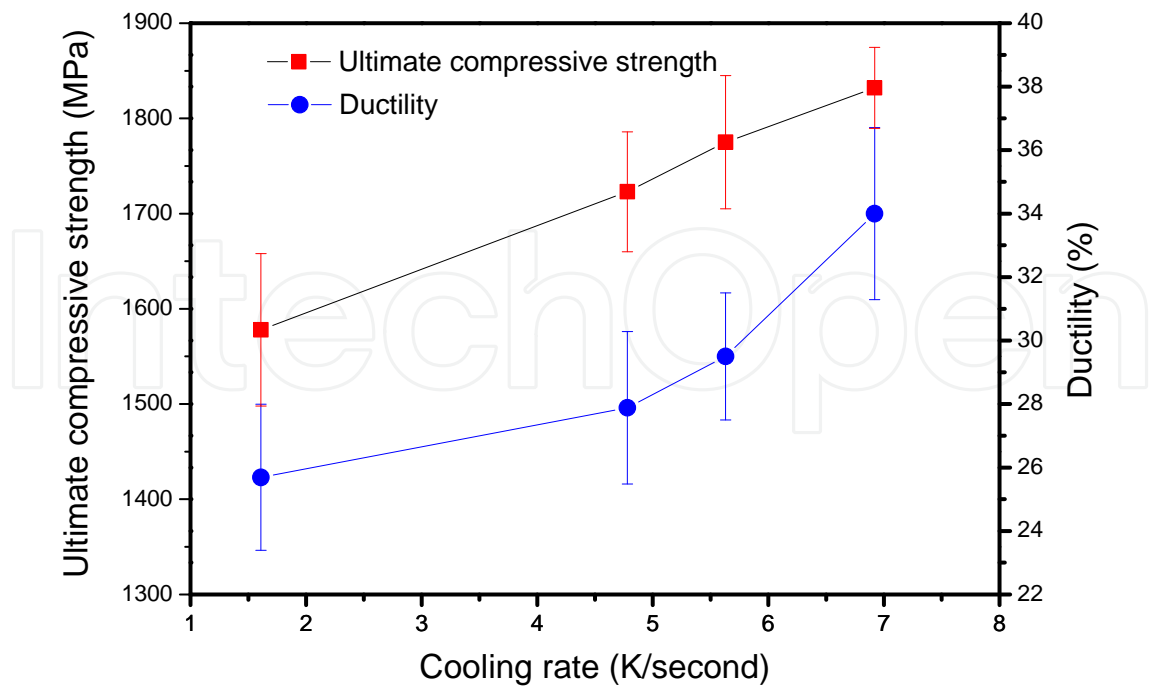

Figure 8. Ultimate compressive strength and ductility of the Ti6Al4V alloys with various cooling rates.

### 3.3. Microstructure of the gas quenched Ti6Al4V alloy

Figure 9 shows the SEM micrographs of the fracture surface of the Ti6Al4V alloys after PECS with various cooling rates. The samples all present a ductile fracture mode with a large amount of plastic deformation undergoing transgranular fracture. However, the fracture surfaces present more and more dimples with increase of the cooling rate (Figure 9a-d). In Figure 9 (d), the sample with cooling rate of 6.9 K/s has much more big dimples and shows more ductile than the sample with cooling rate of 1.6 K/s in Figure 9 (a). It indicates the sample becomes much ductile after the rapid cooling in the PECS. The SEM microstructures are consistent with the mechanical results in Figure 8.
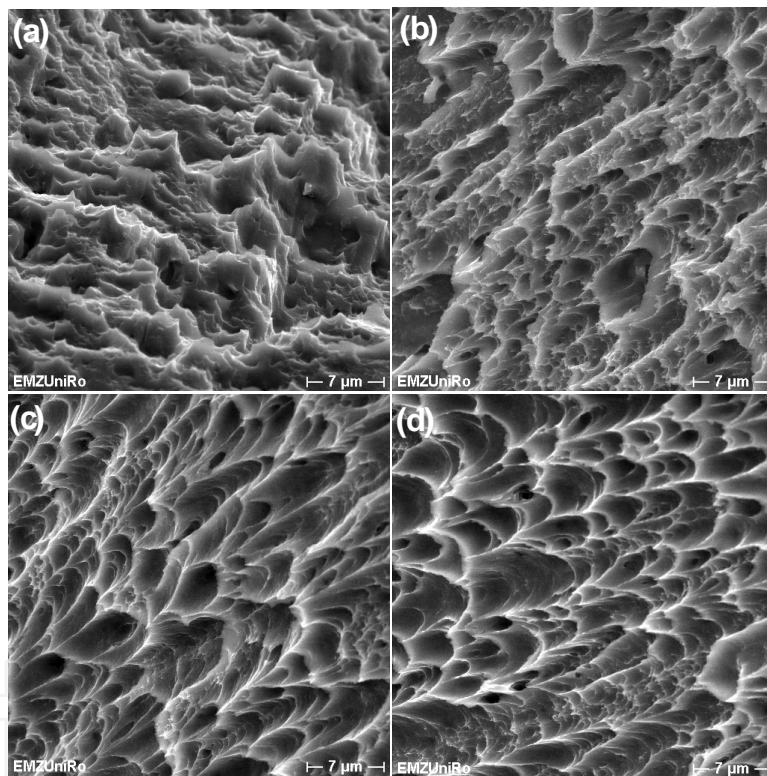
Figure 9. SEM micrographs of the fracture surfaces of the Ti6Al4V alloys with various cooling rates: (a) 1.6 K/s, (b) 4.8 K/s, (c) 5.6 K/s and (d) 6.9 K/s.

Figure 10 provides the metallographic morphology of the Ti6Al4V alloys with various cooling rates. In the etched metallographic images, the β-Ti phase (bcc) appears in white color and α-Ti phase (hdp) in dark color. The samples all show both phases in the microstructures. The microstructures form during sintering at 850°C and subsequent cooling with different rates. On sintering temperature the microstructure consists of a lower amount of α and a higher amount of β. During cooling β partially transforms to α. After

cooling the microstructure consists of former α, retained β and newly formed α. The cooling rate mainly influences on the morphology of the newly formed α. The naturally cooled sample with 1.6 K/s cooling rate shows a relative homogeneous globular $\alpha+\beta$ microstructure (Figure 10a). The rapidly cooled sample shows a different microstructure with a higher fraction of lamellar α phase (Figure 10b). As the cooling rate increases, the 5.6 K/s cooled sample in Figure 10(c) has even more lamellar α phase. In Figure 10(d), the α phase is getting much more lamellar. In general, gas quenching in the SPS resulted in a higher fraction of lamellar α-Ti phase. The XRD results show the gas quenching in the SPS further resulted in the formation of intermetallic phases of $Al_3Ti_{0.8}V_{0.2}$ and Al_2Ti in the alloys [12].
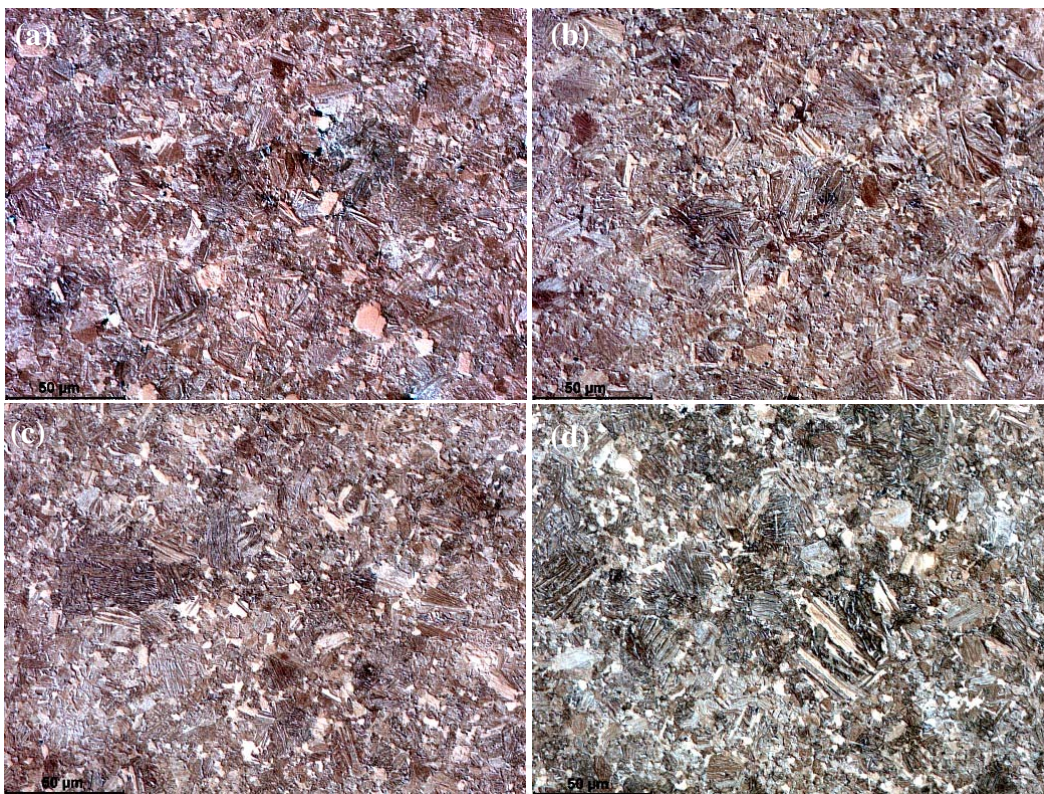
Figure 10. Metallographic micrographs of the surfaces of the Ti6Al4V alloys with various cooling rates: (a) 1.61 K/s, (b) 4.78 K/s, (c) 5.63 K/s and (d) 6.92 K/s.

3.4. Discussions

The cooling power measurments of the Al alloy and steel samples revealed that by the flooding with Ar gas and quenching with N_2 gas can effectively cool the samples. Without graphite dies can cool faster than with graphite dies. The quenching simulation results indicates that the temperature reduced from outside surface of the die gradually to the centre of the sample. At cooling time 100 s, it has about 120 °C temperature gradients from the outside surface of the die to the sample centre.

The hardness, ultimate compressive strength and ductility of the Ti6Al4V alloys have been increased due to the gas quenching. Sinter hardening is applicable for the Ti6Al4V alloy in which the samples are PECS sintered and gas quenched directly after the sintering. It saved energy and costs when compared with a conventional hardening in which the parts must be reheated to the hardening temperature. The microstructures consisted of former α-Ti, retained β-Ti, new α-Ti formed during quenching and intermetallic precipitates. The precipitated nanocrystalline Al_2Ti and $Al_3Ti_{0.8}V_{0.2}$ can play a role of hardening and dispersion reinforcing of the Ti6Al4V alloys. Therefore, the hardness and ultimate compressive strength of the Ti6Al4V alloy are increased. With increasing cooling rate, the newly formed α-Ti becomes more lamellar. The higher fraction of lamellar structured α-Ti phase can lead to the increase in ductility of the Ti6Al4V alloy [13].

The use of industrial gases for quenching high added value parts and offers significant environmental and performance advantages over liquid quenching (water, oil, etc.). Gas quenched parts are clean thus eliminating the need for post-cleaning operations. Due to poor thermal transfer characteristics (lower cooling rate) of gases under normal conditions, they have to be optimized by proper adjustment of gas pressure and flow speed. Gas quenching can be performed in two methods, namely: at low atmosphere pressure with high gas velocity or at high pressure with limited gas velocities [5-8]. In this study, we used the first technique in the PECS that at low or atmosphere pressure with high gas velocity. The flowing rate of the nitrogen gas from nozzles is 8000 l/min. The pressure of gas is only at normal atmosphere pressure. The thermophysical properties of the gas are also an important issue. Based on availability, density and specific heat capacity and thermal conductivity, hydrogen would appear to be good choice as a quench agent [12]. However, because of the explosive risks associated with hydrogen, it is seldom used as a quench gas in commercial heat treating. Nitrogen is the most popular choice, primarily because it is readily available and inexpensive. Argon is used in some special applications but does not quench as effectively as nitrogen and is considerably more expensive. In this study, the PECS vacuum furnace was flooded with argon gas to 40 mbar with the sintering temperature 850 °C being kept, and then quenched with nitrogen gas at high velocity.

The Ti6Al4V alloys have been used in clinic for several decades already. For uncemented knee and hip arthroplasties, Ti6Al4V alloys are the favourable implant materials. Additionally, the Ti6Al4V alloys are preferred for intramedullary rods, spinal clamps, self-drilling bone screws and other implants. One of the main problems of this alloy in biomedical applications is the insufficient ductility which lead to the difficulty in their contouring as required for pelvic and mandibular plates [14]. This investigation indicates that the traditional Ti6Al4V alloy can be modified by PECS with gas quenching leading to various microstructures and mechanical properties. The high ductility of the Ti6Al4V achieved by PECS with gas quenching leads to the easy fabrication of complex shape and plates for the medical applications. The rapid cooling-PECS combining sintering and gas quenching provides a novel method to tailor the microstructure and mechanical properties of the Ti alloys.

4. Pulsed electric current sintering of porous Ti alloys with post heat treatment

4.1. Characterization of raw powders

The Ti6Al4V and NaCl powders are shown in Figure 11. The Ti6Al4V powders have spherical morphologies and size distributions of 5-35 μm. The cuboidal sodium chloride powders have round angles and a size distribution of 125-250 μm. In the preparation process, the size of the metal powder should be smaller than the average powder size of the space holder. By choosing the size, shape and quantity of the space holder material, the mechanical properties of the metal foams can be adjusted [15]. The two kinds of powders were mixed uniformly in a mixer with a small amount of PVA (Polyvinyl alcohol) solution as binder. Then, they were subjected to the PECS machine and sintered at 700 °C under 50 MPa for 8 min in vacuum. Porous Ti6Al4V foams were obtained through dissolution of the NaCl phase in renewed deionized water for 72 h in room temperature. The alloy foams were cleaned in an ultrasonic water bath for 30 minutes and furnace dried at 120 °C for 12 h.
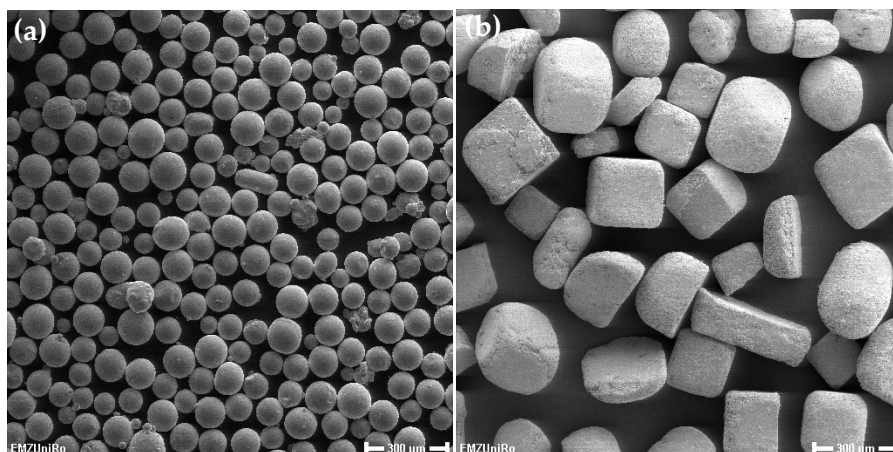
Figure 11. SEM images of the raw Ti6Al4V (a) and NaCl powders (b).

4.2. Post heat treatment by the pressureless PECS

The PECS post heat treatment was used to increase the density and strength of the foams. It was carried out by a pressureless PECS. The set-up of the pressureless PECS is shown in Figure 12. A small gap d in the range of 0–5 mm was designed to avoid damaging the porous materials. The foams after the NaCl being removed were sintered at 1100 °C for 5 min in this pressureless PECS.

## 4.3. Densities and microstructures of the foams

Table 1 shows a summary of the Ti6Al4V foam parameters after PECS. Different weight ratios of NaCl powders were mixed with the Ti6Al4V powders to get various porosities. After

the foams were sintered at 700 °C, they show porosities of 47.6%, 57.6%, 63.9% and 72.5% (±1.0), respectively. When they were post heat treated at 1100 °C, they display porosities of 44.7%, 54.4%, 60.7% and 70.0% (±1.0)%. The porosities decreased and the densities increased after the heat treatment. The densities of the foams have been increased 5.6%, 7.4%, 8.8% and 9.0% at above specific porosities after the heat treatments.

Parameters	3 g Ti6Al4V +1.02g NaCl	3 g Ti6Al4V +1.6 g NaCl	3 g Ti6Al4V +2.2 g NaCl	3 g Ti6Al4V +3.4 g NaCl
Density after PECS at 700 °C (g/cm³)	2.32	1.88	1.60	1.22
Density after heat treatment at 1100 °C(g/cm³)	2.45	2.02	1.74	1.33
Relative density after PECS at 700 °C (%)	52.4	42.4	36.1	27.5
Porosity after PECS at 700 °C (%)	47.6	57.6	63.9	72.5
Relative density after heat treatment at 1100 °C (%)	55.3	45.6	39.3	30.0
Porosity after PECS at 1100 °C (%)	44.7	54.4	60.7	70.0
Increments in density	5.6 %	7.4%	8.8%	9.0%

Table 1. Summary of parameters of the Ti6Al4V foams after PECS.

Detailed microstructural views of the Ti6Al4V foam with 70.0% porosity are shown in Figure 13. Figure 13a and b display the foams fabricated at 700 °C and 50 MPa. They show the porous structure and pore walls, revealing relatively uniformly shaped macropores having rough surfaces, with many micropores (<10 μm) and the shapes and the sizes of the original alloy powders being visible. This indicates that the Ti6Al4V/NaCl mixture is difficult to be densified and, as expected, the diffusion at 700 °C was not sufficient to smooth the micropores due to the very high melting point of Ti6Al4V. Figure 13c and d display the Ti6Al4V foams post heat treated at 1100 °C at a pressureless mode. After the heat treatment, the junctions between the Ti6Al4V powder grains are formed with only few micropores left. As seen in Figure 13d, most of the micropores disappeared due to the heat treatment. This indicates that the pressureless heat treatment contributes to reduce the microporosity of the foams, since no pressure was applied and only diffusion dominated the PECS process. Thus, Ti6Al4V foams with higher density of the walls have been fabricated by the PECS at 700 °C and the post heat treatment at 1100 °C.
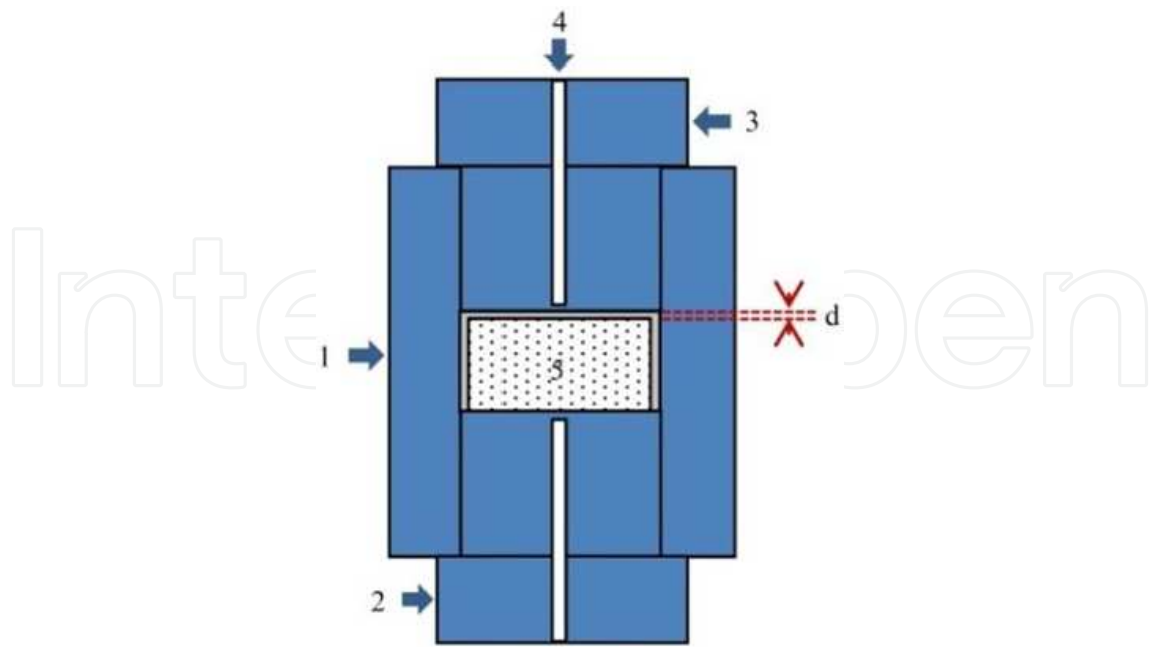
Figure 12. Schematic diagram of the graphite die set-up for the pressureless (1, graphite form; 2, graphite bottom punch; 3, graphite up punch; 4, Pyrometer measurement hole; 5, sample).
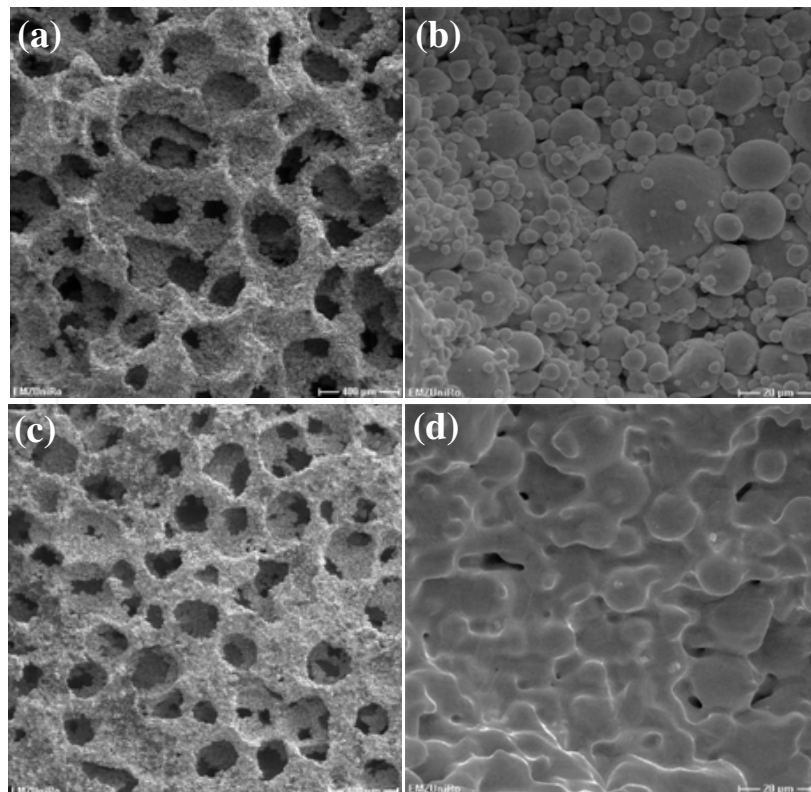
Figure 13. SEM images of the porous structures and pore walls of the Ti6Al4V foams with 70% porosity of the spark plasma sintered at 700 °C and 50 MPa (a, b), and PECS post heat treatment at 1100 °C (c, d).

The outer shape of the Ti6Al4V foam with 54.4% porosity fabricated by the PECS with post heat treatment is shown in Figure 14a. Figure 14b-d shows the micro-CT 3D reconstructions of the foam. The 3D cropped isometric view of cross sections in the Ti6Al4V foam shows the relative uniform pore distribution and interconnected 3D porous structures. The Micro-CT 2D top view and side views show that the macropore shapes are in square cross sections with a relative uniform distribution of pore sizes of 210±40 μm with an average cell wall thickness of 22.1±5 μm.
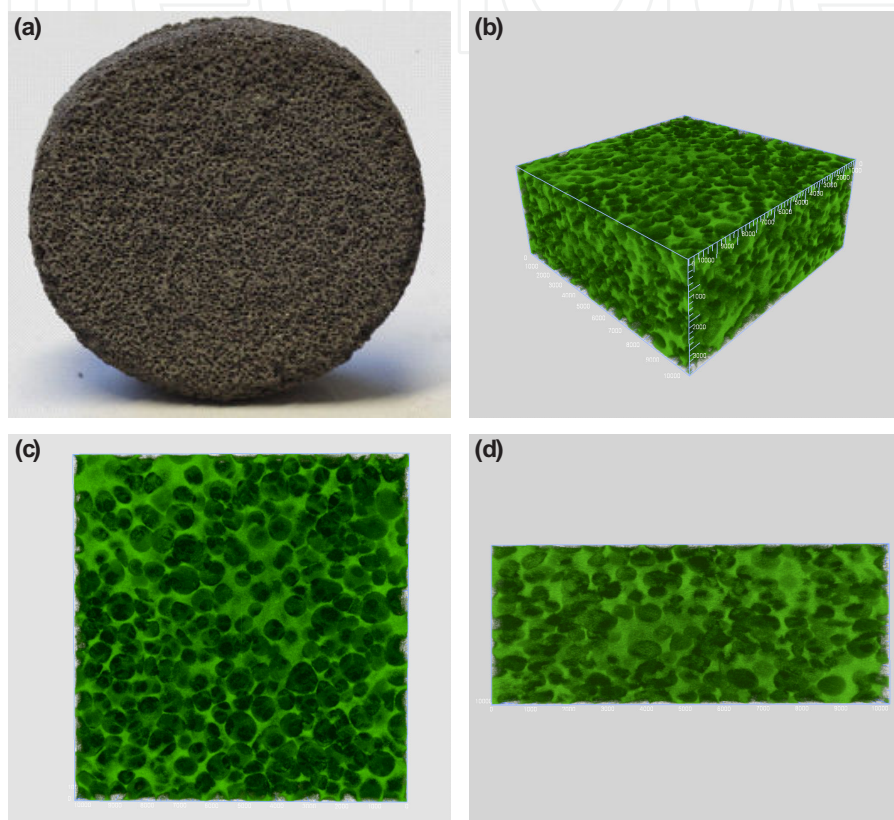

Figure 14. Micro-CT three-dimensional 3D reconstructions of the Ti6Al4V foam (54.4% of porosity) with outer shape of the alloy foam (a), an isometric view (b), top (c) and side view (d).

Figure 15 shows the SEM micrographs of the porous Ti6Al4V foams with different porosities of 44.7%, 54.4%, 60.7% and 70.0% fabricated by the PECS with post heat treatment. SEM images obtained from the porous Ti6Al4V in Figure 15 proved that the space holder NaCl phase was removed completely. The macrostructure of the foam is composed of homogeneously dispersed porous cavities and continuously connected Ti6Al4V struts. It shows mean pores with a size of 150 μm to 250 μm achieved with a NaCl spacer material in the range of 125 μm to 250 μm. The thickness of the pore walls decrease with increasing porosity. The higher porosity samples showed good interconnectivity. The primary pores replicate the size and shape of the angular NaCl particles with rounded corners. Thus, pore shapes can be controlled by using NaCl powders with various shapes. Finally, interconnected pores are visible either as black pores or as necks between adjacent pores in cross sections. These in-

terconnected pores usually ranged 20-150 µm in sizes, indicating that osteoblasts may be able to penetrate into the porous structure.
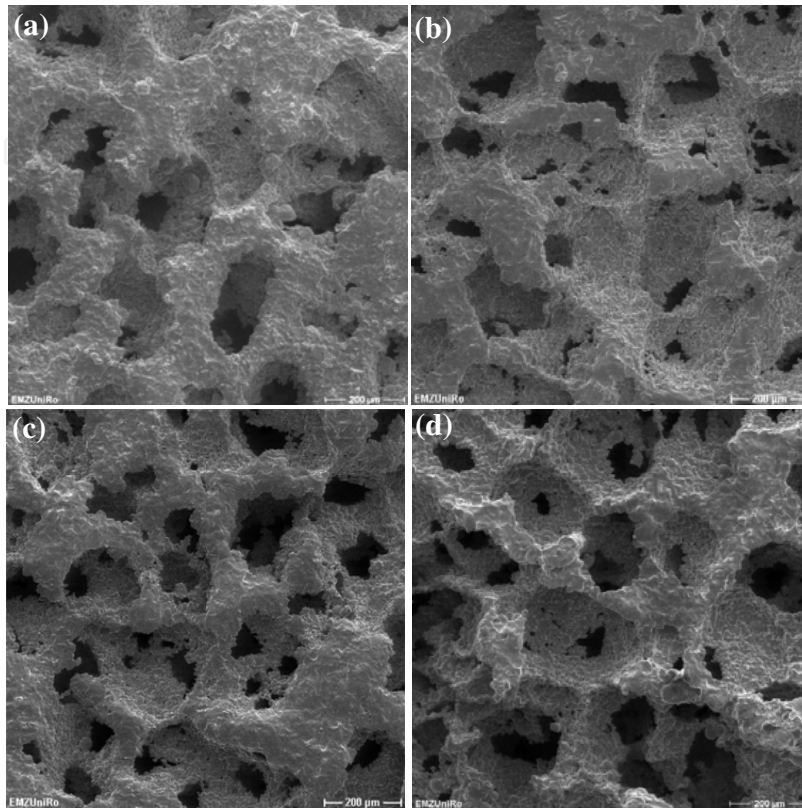
Figure 15. SEM images of the Ti6Al4V foams prepared by PECS with post heat treatment with different porosities of (a) 44.7%, (b) 54.4%, (c) 60.7%, (d) 70.0 %.

4.4. Mechanical properties of the foams

For the evaluation of the mechanical properties of the porous samples, compression tests were performed. Figure 16a shows the Young's modulus and compressive yield strength as a function of relative density for the Ti6Al4V foams and the predicted theoretical values. The Young's modulus of the porous metals is compared with a prediction according to the Gibson and Ashby model [16]:

$$\frac{E}{E_0} = C(\frac{\rho}{\rho_0})^2 \tag{1}$$

where E and E_0 are Young's modulus of foam and bulk materials with densities ρ and ρ_0, respectively, using E_0 = 117 GPa and ρ_0=4.43 g/cm^3 for Ti6Al4V [17]. The proportionality constant C including data of metals, rigid polymers, elasomers, and glasses has to be considered as 1 for titanium alloys [16]. The estimated Young's moduli ranging from 34.11GPa to

9.84GPa obey exponential decays with the increase of porosity, and the actual measured Young's moduli of the foams are comparable with the calculated Young's modulus based on the density of the Ti6Al4V foam. Besides the Young's modulus, the strength is an important property of orthopedic implants, in particular in load bearing applications. According to the Gibson-Ashby model, the relationship between the yield strength and relative density is given by [16]:

$$\frac{\sigma}{\sigma_0} = C(\frac{\rho}{\rho_0})^n \tag{2}$$

where σ_0 and ϱ_0 are the yield strength and the density of the solid material, σ and ϱ of the foam, respectively. The experimental data indicate that C from the data of cellular metals and polymers is around 0.3 and the strength of the foam is proportional to the strength of the solid (n = 3/2) [18]. The density of dense solid Ti6Al4V is 4.43 g/cm^3 with yield strength 902 MPa [19, 20]. The yield strength of Ti6Al4V foams and predicted theoretical values for open porous material are given in Figure 16b. It can be seen that the measured values for porous Ti6Al4V are slightly higher than the analytical predictions by Gibson and Ashby for open structures, also much higher than the compressive strength of cancellous bone (10-50MPa). The experimental values are all comparable with the calculated data obeying the Gibson and Ashby model.
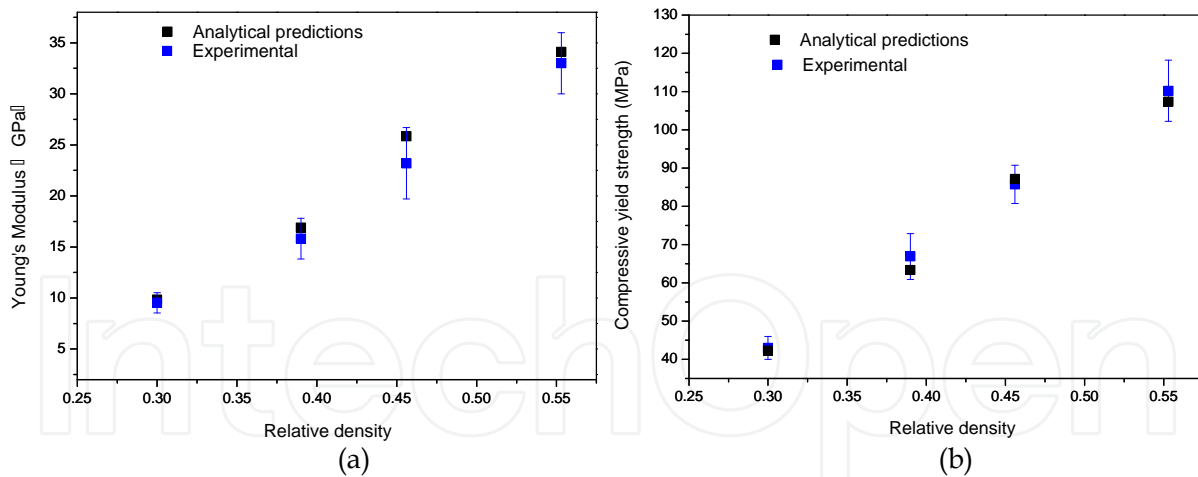
Figure 16. Young's modulus (a) and yield strength (b) of the Ti6Al4V foams and theoretically predicted values.

Figure 17 shows the SEM images of the Ti6Al4V foams (44.7%porosity) after the compressive tests. The macropores have been compressed to a crushed shape. However there were no bulk cracks been oberserved. By this way, it can adsorbe a large amount of energy. The strength of the foams depends on the thickness of the struts. The 44.7%porosity foam has the largest yield strength and Young's modulus (Figure 16) due to the the thickest struts in this group of the prepared samples.
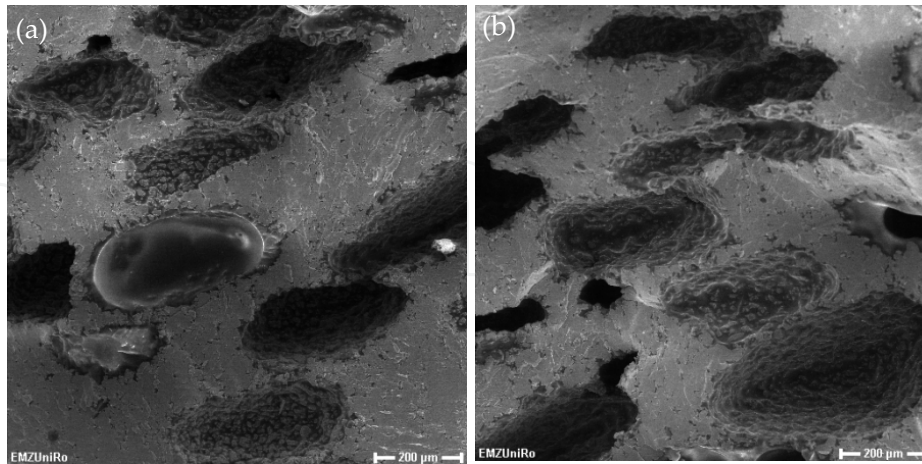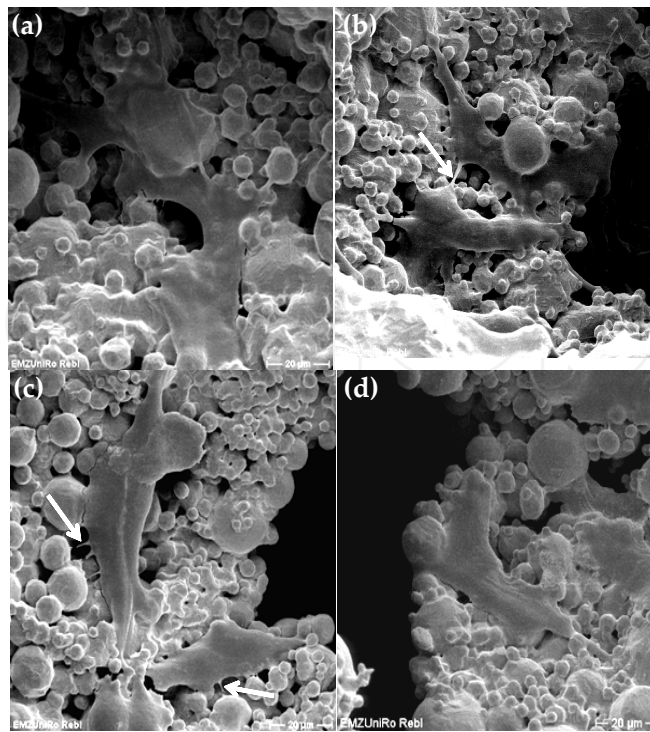
Figure 17. SEM images of the Ti6Al4V foams (44.7%porosity) after the compressive tests showing the crushed shape pores of different places (a) and (b).

4.5. Cell proliferation in the foams

Human osteoblast like cells (MG-63) were cultured on the porous Ti6Al4V samples. Figure 18 shows the SEM images of human bone-like MG-63 cells on porous Ti6Al4V foams with 44.7%, 54.4%, 60.7%, and 70.0 %. After 24 h they exhibit a well spread morphology and excellent bonding to the surface. The cells form filopodia to reach the adjacent grains of the Ti6Al4V structure. The cells grow inside the pores to a large extend implying a good integration when implanted into the bone. For a better interconnectivity, higher porosity Ti6Al4V foams (above 60%) are recommended for the biomedical applications. This cell tests display that the pore sizes and porous surface of the Ti6Al4V foams fabricated by the PECS are suitable for the osteoblasts in-growth.

4.6. Other methods for preparation of Ti6Al4V foams by PECS

Besides NaCl particles as spacer material, some other ways to fabricate Ti foams by the SPS were also tried and studied. Fig.19 shows the SEM images of the Ti6Al4V foams prepared by SPS using Cu spacer. The Ti6Al4V powders and Cu powders were mixed and sintered by PECS at 800 °C and 50 MPa for 5 min holding time. Then the Cu spacers were removed by high concentration HNO_3 acid washing. Finally, they were washed in deioned water to get a neutral PH value. The porous foams were obtained. The porous structures at various magnifications show that the pores are interconnected with pore sizes from 10 to 200 micrometers. The pore walls show that there are many TiO_2 nanostructures formed on the surfaces. Its formation is due to the strong acid oxidation. The TiO_2 nanostructures could increase the bioactivity and cell adhesion property of the Ti6Al4V foams.

**Figure 18.** SEM of human bone-like MG-63 cells on porous Ti6Al4V foams (a) 44.7%, (b)54.4%, (c) 60.7%, (d) 70.0 %. The cells display a well spread morphology and moreover the cells extend various filopodia to the adjacent grains (arrow).
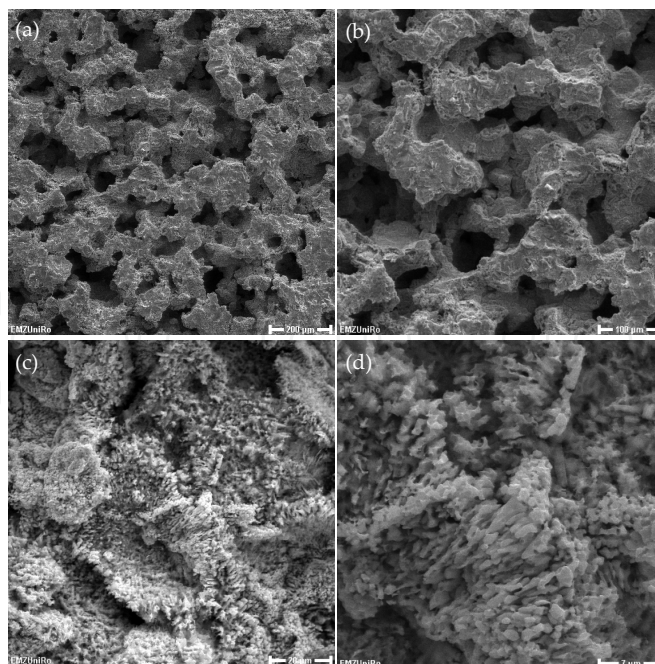
Figure 19. SEM images of the Ti6Al4V foams prepared by the PECS using Cu spacer: (a,b) porous structure at various magnifications, and (c,d) pore walls showing the TiO$_2$ nanostructures.

Another method to prepare the Ti foams is by the simulated body fluid soaking of the sintered TiMg solids. It is an in-situ pore formation method. The TiMg solids were prepared by ball milling of Ti and Mg powders and PECS at 600 ºC and 50 MPa for 5 min. Figure 20(a) shows the XRD diffraction results of the TiMg solids with 10-40 wt% fraction of Mg. It exhibits pure Ti and Mg phases, no intermetallic phases. Afterwards, they were immersed in the simulated body fluid for several weeks. Figure 20 (b) exhibits the surface of the Ti-40 wt %Mg solids before the body fluid soaking. Figure 20 (c) shows the in-situ formed macropores after 4 weeks soaking in the simulated body fluid. The pore sizes are about 500-700 μm in dimension. The pore wall in Figure 20(d) shows the microstructures after body fluid soaking and some hints of corrosions can be found. The dense TiMg solids can load higher forces than the porous Ti foams. After they were implanted *in vivo*, the Mg composition in the TiMg solids will be degraded by body fluid immersion to form porous foams with time going. The bone tissue would grow into the foams simultaneously with the pore forming progress. The degradation rate can be tailored by the fraction of Mg and the alloying elements in the Mg phase.
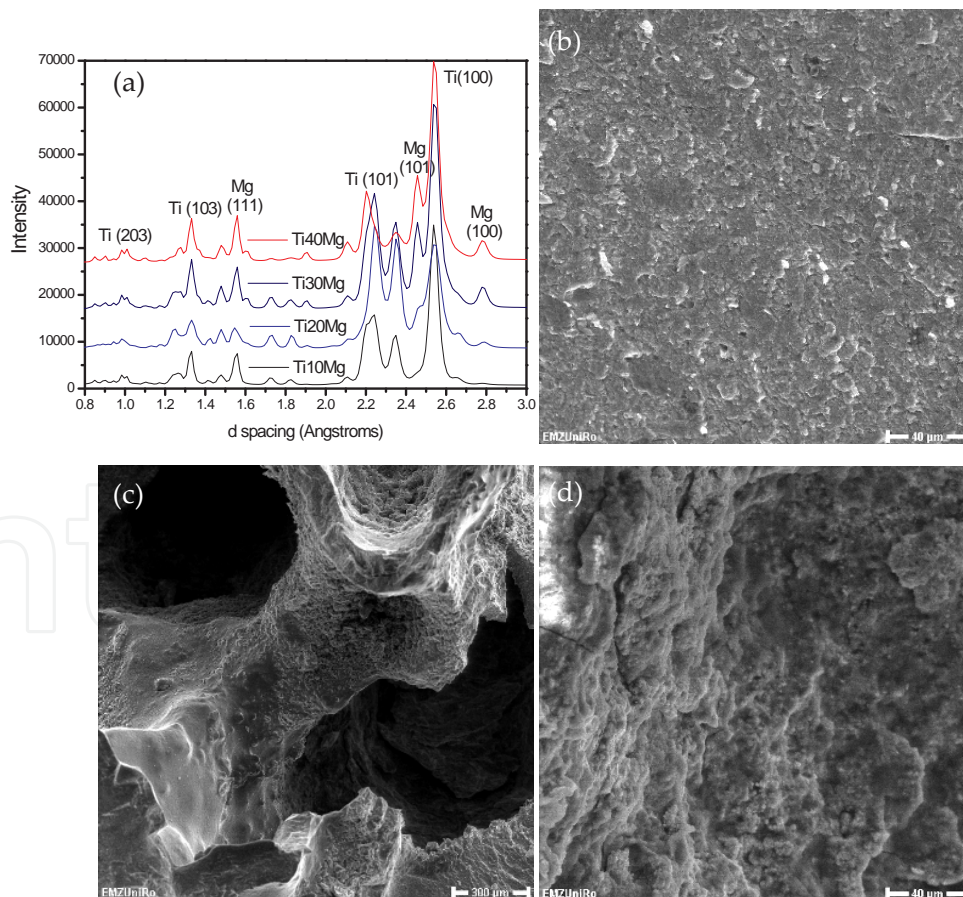
Figure 20. XRD results of the SPS prepared TiMg system (a) and SEM images of the Ti40Mg solid surface (b), in-situ formed macropores in the simulated body fluid (c) and pore wall structure (d).

4.7. Discussions

In this study, the Ti6Al4V foams were fabricated by using PECS at controlled porosity followed by dissolution of NaCl phase and post heat treatment at 1100 °C. Previous investigations showed that high-density pure Ti foams can be fabricated with NaCl as spacer by the PECS at 700 °C for 8 min under 50 MPa [11]. However, the Ti6Al4V/NaCl mixture cannot be densified at the same condition. It indicates that the Ti6Al4V/NaCl mixture is difficult to be consolidated either in the hot pressing [10] or in the PECS. The pressureless PECS method was firstly proposed by Zhang et al [21]. It can be used for the preparation of ceramic nanoscaffolds and for other inorganic porous materials [21, 22]. The Ti6Al4V foams were post heat treated by the pressureless PECS method at 1100 °C for 5 min. The densities of the foams have been increased from 5.6 to 9.0% at various porosities (Table 1). The relative density values calculated by dividing the mass of the samples by the volume can provide the information of macroporosity and microporosity in the foams. The macroporosity has been determined by the fraction of NaCl spacer after the PECS at 700 °C and dissolution in water. The post heat treatment by pressureless PECS at 1100 °C will contribute to reduce the microporosity of the foams. During the heat treatment by the pressureless PECS, there was no pressure being applied, therefore the surface diffusion, volume diffusion and grain boundary diffusion dominated the PECS process. These diffusions mainly play roles of reducing the microporosities in the foams. The SEM results in Figure 13a-d validated this scientific assumption. This post heat treatment by the pressureless PECS is similar to the technique of hot isostatic pressing (HIP) used to reduce the microporosity of metals and to increase the density of many ceramic materials, thus improving the material's mechanical properties. The post heat treatment by the pressureless PECS can be done in vacuum and argon gas up to 40 hPa. The results in this study indicate that this pressureless PECS method can be used for post heat treatment of Ti6Al4V foams, and possibly for all the metallic foams, dense metals and ceramics.

This method using PECS by dissolution of NaCl spacer and post heat treatment provides a foamed structure with a close to homogenous pore structure, high levels of porosity and high mechanical properties. The mechanical properties of the metal foam can be adjusted by choosing the size, shape and quantity of the space holder material used. Besides the NaCl as spacer material, Cu also can be used as a spacer material to get Ti6Al4V foams. It can modify the surface of the foams simultaneously with TiO_2 nanostructures. The key point of this method is how to get rid of the Cu completely. The in-situ pore forming method is very interesting. The Mg spacer degraded in the body fluid and generated some pores in the sintered TiMg solids. The key issue of this method is how to match the growth rate of the bone tissue. It can be realized by tailoring the fraction of Mg in the Ti alloy and the alloying elements in the Mg phase (e.g. Zr, Ag etc.). The highly porous nature of the alloys combining good mechanical properties with osteoconductivity makes these materials ideal for bone scaffolds. The future highlights will be net-shape processing of foams with complex forms by the PECS method. Prospectively, this kind of Ti6Al4V foams is potential to alleviate the problem of mechanical mismatch between the bone and the Ti alloy implant and may provide a new candidate as a long-term bone substitute for biomedical applications.

5. Conclusions and outlook

The pulsed electric current sintering was modified and equipped with a novel nitrogen gas rapid cooling system. The cooling power of the system was measured and numerical simulated using the Al-2024 and ALSI303 steel as model materials. The argon gas flooding and nitrogen gas quenching can effectively cooling the samples and increase their heat transfer coefficient. The Ti6Al4V alloys were prepared with various cooling rates ranged from 1.6 to 6.9 K/s by changing the thickness of the graphite dies. The gas quenching has increased the hardness, ultimate compressive strength and ductility of the Ti6Al4V alloy from 327 HV1, 1578 MPa, and 27.4% up to 353 HV1, 1832 MPa and 34%, respectively. The rapid cooling leads to much more pronounced dimples in fracture surfaces, precipitation of intermetallic phases ($Al_3Ti_{0.8}V_{0.2}$ and Al_2Ti), and more lamellar α-Ti phase in metallography. The rapid cooling-PECS combining sintering and gas quenching provides a novel method to tailor the microstructure and mechanical properties of the Ti alloys.

The Ti6Al4V foams were fabricated by the PECS with post heat treatment using a blend of Ti6Al4V and sodium chloride powders. The Ti6Al4V foams fabricated at 700 °C and 50 MPa in PECS cannot achieve high relative densities. The sintered foams were post heat treated in a pressureless mode of the PECS at 1100 °C for 5 min. This heat treatment is very effective to reduce microporosity and to fully densify the foam walls. Young's moduli of the foams were in the range of 33.0 GPa to 9.5 GPa and the yield strengths ranged from 110.2 MPa to 43.0 MPa with porosity values from 44.7% to 70.0% obeying the Gibson-Ashby models. The macropores have been crushed to flat shapes without cracks. The human osteoblast cell line MG-63 validated the cellular acceptance of the foam surfaces. This pressureless PECS method can be used for post heat treatment of Ti6Al4V foams. The Ti6Al4V foams with Cu spacer were prepared by the PECS. There pore walls were modified with TiO_2 nanostructures. The in-situ pore forming method by soaking of the TiMg solids in the simulated body fluid was also introduced.

In this century, worldwide energy shortage is a serious problem for humankind. Therefore, how to save energy is a hot issue in industry and our everyday life. The PECS is a relative new sintering technique with rapid energy transfer and less energy consumption to produce advanced materials. It is considered as a novel field assisted sintering technique for fast preparation of diverse bulk materials (metals, ceramics, polymers and their composites) with a near net shape. The sinter hardening by the PECS, in which the parts are sintered and quenched directly after the sintering step, has a perspective future in the PM industry due to energy saving and cleanness. The post heat treatment of materials in the pressureless PECS possibly should be suitable for all the porous materials and dense solids. The in-situ pore forming method represents the tendency of the future in the field of cellular solids. In the end, the future highlights will focus on the preparation of nanostructured materials and composites by the PECS with gas quenching and the computer simulation of the gas quenching process in the PECS, as well as the processing of porous nanofoams by the pressureless PECS with complex shapes.

Acknowledgements

Author details

F. Zhang[1], Y. Quan[1], M. Reich[2], O. Kessler[2] and E. Burkel[1]

1 Chair of Physics of New Materials, University of Rostock, Rostock, Germany

2 Chair of Materials Science, University of Rostock, Rostock, Germany

References

[1] Zhang F., Burkel E. Novel titanium manganese alloys and their macroporous foams for biomedical applications prepared by field assisted sintering. In: Anthony N. (ed.) Biomedical Engineering, Trends, Researches and Technologies. Rejeka: InTech; 2011. p 203-224.

[2] Zhang F., Burkel E. Synthesis of diamond using spark plasma sintering. In: Lakshmana A. (ed.) Sintering of Ceramics - New Emerging Techniques. Rejeka: InTech; 2012. p 27-58.

[3] Dlapka M., Danniger H., Gierl C., Lindqvist B.. Sinter hardening-a special heat treatment for powder metallurgy precisions parts. Journal of Heat Treatment and Materials 2012; 67(3) 223-231.

[4] Thakuc S. N., Newkirk J. W, Fillari G.B., Murphy I.F. and Narasimhan K.S. Mechanical Properties of Sinter-Hardened Steels. International Journal of Powder Metallurgy. 2004; 40(3) 45-54.

[5] Reich M., Schöne S., Keßler O., Nowak M., Grydin O., Nürnberger F., Schaper M. Simulation of gas and spray quenching during extrusion of aluminium alloys, Key Engineering Materials. 2010; 424: 57-64.

[6] Schöne S., Reich M., Keßler O. Integration des Gasabschreckens in das Strangpressen von Aluminiumlegierungen - eine Machbarkeitsstudie, HTM Journal of Heat Treatment and Materials. 2011; 66 (3):175-181.

[7]   Schöne S., Reich M., Keßler O., Gas nozzle field quenching of L-shaped aluminium extrusion profiles, Proc. 3rd International Conference on Distortion Engineering 2011, Sept 14-16, 2011, Bremen, Germany, 75-82

[8]   Reich M., Kessler O. Numerical and experimental analysis of residual stresses and distortion in different quenching processes of aluminum alloy profiles, Proc. 6th Int. Quenching and Control of Distortion Conf., 9.-13.9.2012, Chicago, IL, USA, Ed. D. Scott MacKenzie, ASM International, 2012, 563-574.

[9]   Dunand D.C. Processing of titanium foams. Advanced Engineering Materials 2004; 6(6): 369-376.

[10] Ye B, Dunand D. C. Titanium foams produced by solid-state replication of NaCl powders. Materials Science and Engineering A 2012; 528 691-697.

[11] Zhang F., Otterstein E., Burkel E. Spark plasma sintering, microstructures and mechanical properties of macroporous titanium foams. Advanced Engineering Materials. 2010, 12 (9): 863-872

[12] Zhang F., Reich M., Quan Y., Kessler O., Burkel E. Preparation and characterization of Ti6Al4V alloys by spark plasma sintering with integrated gas quenching. Journal of the Mechanical Behavior of Biomedical Materials.(Accepted)

[13] Kim J.H., Semiatin S.L., Lee C.S. Constitutive analysis of the high-temperature deformation of Ti–6Al–4V with a transformed microstructure. Acta Materialia 2003,51:5613-5626.

[14] Zhou Y. L., Niinomi M., Akahori Toshikazu T. Changes in mechanical properties of Ti alloys in relation to alloying additions of Ta and Hf. Materials Science and Engineering A. 2008; 483–484: 153–156

[15] Quan Y, Zhang F., Rebl H., Nebe B. Kessler O., Burkel E.Ti6Al4V foams fabricated by spark plasma sintering with post heat treatment. Materials Science and Engineering A. 2012, doi 10.1016/j.msea.2012.12.026

[16] Gibson L. J., Ashby M. F. Cellular Solids: Structure and Properties 2nd , Cambridge; 1997. p175–281.

[17] Choe H., Abkowitz S.M., Abkowitz S. and Dunand D.C. Effect of Tungsten Additions on theMechanical Properties of Ti-6Al-4V. Materials Science and Engineering A 2005; 396: 99-106.

[18] Biener J., Hoodge A. M., Hamza A. V., Hsiung L. M. and Satcher J. H., Nanoporous Au: A high yield strength material. Journal of Applied Physics 2005; 97: 024301.

[19] Bram M., Schiefer H., Bogdanski D., Koller M., Buchkremer H. P., Stover D. Implant surgery: How bone bonds to PM titanium. Metal Powder Report 2006; 61 (2) 26-28.

[20] Lee M. H., Kim K. B., Han J. H., Eckert J., Sordelet D. J. High strength porous Ti–6Al–4V foams synthesized by solid state powder processing. Journal of Physics D: Applied Physics 2008; 41: 105404.

[21] Zhang F., Lin K., Chang J., Lu J. and Ning C. Spark plasma sintering of macroporous calcium phosphate scaffolds from nanocrystalline powders. Journal of the European Ceramic Society. 2008; 28: 539-545.

[22] Ibrahim A., Zhang F., Otterstein E., Burkel E. Processing of Porous Ti and Ti5Mn Foams by Spark Plasma sintering. Materials and Design. 2011; 32: 146-153.